Scientia Psychiatrica
Vol. 7, No. 2, 2026, pp. 86–98 · e-ISSN 2715-9736 journal homepage: scientiapsychiatrica.com

ORIGINAL RESEARCH ARTICLE

Dorsolateral Prefrontal Cortex Co-expression Modules and Cell-Type Composition in Major Depressive Disorder and Suicide

Akmal Hasan[1*], Jason Willmare[2]
[1]*Department of Neurology, Phlox Institute, Palembang, Indonesia*
[2]*Department of Neurology, Diffa State Hospital, Diffa, Niger*

ARTICLE INFO

Article history
Received: April 26, 2026
Revised: March 25, 2026
Accepted: April 20, 2026
Available online: April 27, 2026
Published: April 30, 2026

Keywords
Cell composition
Dorsolateral prefrontal cortex
Major depressive disorder
Single-nucleus RNA sequencing
Suicide
Weighted gene co-expression network analysis

***Corresponding author**
Akmal Hasan
E-mail: Akmal.hasan@phlox.or.id
ORCID: 0009-0009-8051-7299

DOI
10.37275/scipsy.v7i2.212

ABSTRACT

Background. Major depressive disorder (MDD) and death by suicide may involve transcriptional and cellular shifts in the dorsolateral prefrontal cortex (DLPFC). Bulk transcriptomes mix within-cell regulation with tissue composition, so signals may not reproduce.

Objective. To identify covariate-adjusted DLPFC co-expression modules associated with MDD and suicide, relate them to cell-type signatures, and assess external reproducibility.

Methods. This secondary analysis of public datasets used GSE101521 (29 controls, 21 MDD donors who died by suicide [MDD-S], and 9 who died otherwise [MDD-NS]). After covariate residualization, the 5,000 most variable genes entered signed weighted gene co-expression network analysis. Eigengenes were tested with empirical-Bayes models and false-discovery rate (FDR) correction. GSE144136 supplied cell signatures and donor-level composition; scores were tested in 15 matched GSE54568 pairs.

Results. The brown module (509 genes; inflammatory enrichment) was nominally lower in MDD ($\beta = -0.499$; $p = 0.045$; FDR = 0.316) and MDD-S ($\beta = -0.570$; $p = 0.039$; FDR = 0.274) than controls; blue showed the largest MDD-S versus MDD-NS estimate ($\beta = -0.807$; $p = 0.015$; FDR = 0.105). No module or bulk-deconvolved cell fraction reached FDR < 0.05. In GSE144136 (male donors), MDD-S showed lower relative astrocyte (FDR = 0.002) and higher excitatory and inhibitory neuronal (both FDR = 0.024) composition. No module replicated in GSE54568; two of five were directionally concordant.

Conclusion. Inflammatory and oligodendrocyte-related modules lacked multiplicity-adjusted or external support for phenotype associations. Donor-level composition gave stronger yet constrained evidence. The findings prioritize immune-glial and neuronal hypotheses for replication, not biomarker use.

Copyright: © 2026 The Author(s). Published by HM Publisher in collaboration with CMHC Research Center on behalf of Scientia Psychiatrica. The authors retain copyright of their work.

Access licence: This is an open access article distributed under the terms of the Creative Commons Attribution–NonCommercial–ShareAlike 4.0 International Licence (CC BY-NC-SA 4.0), which permits non-commercial use, sharing, adaptation and reproduction in any medium, provided the original author and source are credited and any derivative work is distributed under the same licence.

1. Introduction

Major depressive disorder (MDD) is a heterogeneous syndrome. It shows itself through affective, cognitive, somatic, and behavioral symptoms. Post-mortem brain studies expose this heterogeneity clearly, because one diagnostic label can cover very different illness durations, symptom trajectories, treatments, comorbidities, causes of death, and agonal circumstances. Suicide adds a further layer. MDD is a major clinical setting for suicidal behavior, yet death by suicide is not interchangeable with depression, and its molecular correlates may reflect acute state, method of death, toxicological exposure, stress physiology, or mechanisms that cut across diagnostic boundaries. A transcriptomic design should therefore keep the general MDD contrast apart from comparisons involving suicide status, instead of treating the two as a single phenotype. The dorsolateral prefrontal cortex (DLPFC), including Brodmann area 9, is a plausible region for studying these distinctions. It supports executive control, working memory, cognitive flexibility, valuation, and top-down regulation of emotion. MDD commonly alters these functions. They also bear on the cognitive constriction, poor problem solving, and changed decision processes that can accompany a suicidal crisis. Still, a post-mortem DLPFC signal does not read out one psychological process. It is a composite of neuronal and non-neuronal expression,

vascular and immune states, cell proportions, tissue preservation, lifetime exposures, and the terminal interval. Careful multivariable adjustment and cautious interpretation are both essential.

Earlier bulk and single-nucleus work showed that depression and suicide involve more than a handful of differentially expressed genes. The original report on the discovery RNA-sequencing cohort described glial, endothelial, immune, chemokine, and ATPase-related alterations, and the cell-reference cohort pointed to oligodendrocyte precursor cells and excitatory neurons in MDD DLPFC.[1,2] In 2022, studies widened the picture to the genetics of completed suicide,[3] cortico-amygdala circuitry,[4] state and trait molecular structure,[5] oligodendrocyte oxidative stress,[6] prefrontal suicide signatures,[7] connectome gradients,[8] and transcriptomic aging.[9] No single universal molecular lesion emerges from this body of work. It argues instead for analyzing coordinated systems while paying explicit attention to tissue and cohort composition.

Gene co-expression network analysis tackles part of this problem. It groups genes that covary across samples and summarizes each group with an eigengene. Modules cut the burden of thousands of gene-wise tests, expose coordinated biology, and yield a reproducible weighted gene set for external evaluation. Biological coherence, however, does not show that a module differs by diagnosis. A stable cell-type program present in every donor can produce strong pathway enrichment. A nominal eigengene association, in turn, can fail to reproduce in an independent cohort. Defining a module, testing its association with phenotype, annotating its function, and reproducing it externally are four separate evidential steps. Cellular composition is a second major axis of interpretation. Bulk RNA sequencing averages RNA over neurons, astrocytes, oligodendrocytes, oligodendrocyte precursor cells (OPCs), microglia, endothelial cells, and other populations. A bulk module may therefore reflect altered regulation inside one cell type, a shift in the relative amount of that cell type, or both, and studies from 2023 showed that neuroimmune signatures,[10] cortical transcriptional gradients,[11] brain structure-function associations,[12] single-nucleus stress responses,[13] sex- and symptom-related profiles,[14] and suicide-dependent targets[15,16] differ widely between cohorts and analytical scales. Single-nucleus RNA sequencing (snRNA-seq) provides reference profiles for computational deconvolution. Deconvolution, though, carries signatures from one assay to another and returns relative RNA contributions, not histological cell counts. Direct snRNA-seq proportions stay compositional too. Nucleus isolation, recovery, cluster annotation, cortical layer sampling, and case-control differences in nuclear quality can all distort them.

Work from 2024 identified sex- and suicide-specific kynurenine changes,[17] shared post-mortem mechanisms,[18] temporally patterned expression,[19] imaging-linked gene signatures,[20] and altered hippocampal transcriptomes and cell composition.[21] Larger studies in 2025 followed. They reported convergent excitatory-neuron pathways,[22] cell-specific programs of depression and suicide risk,[23] purinergic changes,[24] regional suicide phenotypes,[25] single-cell stress dynamics,[26] multi-omic orbitofrontal profiles,[27] late-life depressive signatures,[28] blood co-expression modules,[29] and post-mortem MDD networks.[30] Single-nucleus and multi-omic reports from early 2026 again stress cell-type specificity and partial overlap across disorders.[31,32] Such a moving evidence base explains why orthogonal replication is needed. Dynamic range, feature coverage, preprocessing, tissue sampling, and phenotype definitions can each change the result. External validation should apply locked discovery information, report mapping loss, assess direction and uncertainty, and refrain from rebuilding modules in the validation data.

This study combines three public DLPFC datasets, each with its own role. GSE101521 offers a bulk RNA-sequencing discovery cohort with three groups: controls, MDD who died by suicide (MDD-S), and MDD who died from other causes (MDD-NS). GSE144136 offers control-derived cell-type signatures and donor-level observed nuclear composition for male MDD-S cases and controls. GSE54568 offers matched microarray pairs for a cross-platform test of discovery-weighted module scores. The analytical hierarchy keeps the primary MDD contrast separate from suicide-related secondary contrasts. It also keeps cell-marker enrichment separate from inferred or observed composition. What is new here is the joint, replication-aware evaluation of covariate-adjusted DLPFC co-expression, control-derived cell-type annotation and deconvolution, direct donor-level nuclear composition, and locked-weight external module scoring across complementary datasets. Pathway enrichment is not treated as disease association, and direct nuclear proportions are not treated as absolute cell counts. The design keeps these layers apart and reports multiplicity-adjusted and externally non-replicated findings as exactly that. The aim was to identify DLPFC co-expression modules associated with MDD and suicide status, to relate those modules to cell-type composition, and to evaluate their external reproducibility.

2. Methods

2.1. Study design and reporting framework

This was a secondary, observational, multi-cohort analysis of publicly available post-mortem transcriptomic data. The design assigned one analytical role to each dataset before interpretation: GSE101521 for bulk discovery, GSE144136 for cell-reference construction and direct donor-level composition, and GSE54568 for external validation. The donor was the unit of biological inference. Nuclei, genes, and microarray probes were measurement units and were not treated as independent human observations. Reporting followed relevant principles of the Strengthening the Reporting of Observational Studies in Epidemiology (STROBE) guideline lfor observational studies and incorporated transcriptomic-specific information on preprocessing, covariates, multiplicity, mapping, and validation.

The primary estimand was the adjusted standardized difference in each discovery module eigengene between all donors with MDD and controls. Planned secondary estimands compared MDD-S with controls, MDD-NS with controls, and MDD-S with MDD-NS. Pathway enrichment, cell-marker enrichment, bulk deconvolution, observed snRNA-seq composition, and external module scoring were complementary analyses; none was used to retroactively redefine the primary outcome. Statistical evidence was judged primarily by multiplicity-adjusted false-discovery rate (FDR), with nominal p values used only to identify hypotheses for replication.

2.2. Datasets and participants

GSE101521 comprised bulk RNA sequencing of DLPFC Brodmann area 9 (BA9) from 59 donors: 29 non-psychiatric controls, 21 donors with MDD who died by suicide, and 9 donors with MDD who died from causes other than suicide.[1] The control group included 6 women (20.7%), the MDD-NS group included 3 women (33.3%), and the MDD-S group included 8 women (38.1%). Mean ages were 43.5 years (SD 21.3), 57.7 years (SD 15.5), and 52.0 years (SD 21.7), respectively. Median RNA integrity numbers were 7.03, 7.38, and 6.61; corresponding mean post-mortem intervals were 13.2, 15.1, and 16.1 hours, and mean brain pH values were 6.49, 6.41, and 6.41. Seven donors were younger than 18 years, motivating an adult-only sensitivity analysis.

GSE144136 comprised snRNA-seq data from DLPFC Brodmann area 9 in 17 male controls and 17 male donors with MDD who died by suicide.[2] The dataset was used in two non-equivalent ways. First, nuclei from control donors alone supplied cell-type expression signatures for deconvolution of GSE101521 bulk tissue, reducing leakage of case-associated expression into the reference. Second, the observed distribution of annotated nuclei was summarized for each donor and tested directly. Because all cases were MDD-S and all donors were male, this comparison cannot isolate diagnosis from suicide status or establish applicability to female donors.

GSE54568 comprised Affymetrix GPL570 measurements from DLPFC Brodmann area 9 in 15 matched MDD-control pairs. It served as a deliberately stringent external evaluation because the assay platform differed from discovery, and the validation target was not a newly fitted network but the score of genes and weights defined in GSE101521; the three datasets, their analytical roles, and their principal inferential limits are detailed in Table 1.

Table 1. Datasets, participants, analytical roles, and principal limits.

Role	Dataset and assay	Participants	Purpose and principal limit
Discovery	GSE101521; bulk RNA-seq, DLPFC BA9	29 controls; 21 MDD-S; 9 MDD-NS	Network construction and adjusted phenotype contrasts; MDD-NS n = 9
Cell reference	GSE144136; snRNA-seq, DLPFC BA9	17 male controls; 17 male MDD-S	Control-only signatures and observed donor composition; diagnosis, suicide, and sex cannot be separated
External evaluation	GSE54568; Affymetrix GPL570, DLPFC BA9	15 matched MDD-control pairs	Locked discovery-weighted module scores; cross-platform mapping and non-equivalent phenotype detail

Notes: BA9, Brodmann area 9; DLPFC, dorsolateral prefrontal cortex; MDD, major depressive disorder; MDD-NS, MDD who died from causes other than suicide; MDD-S, MDD who died by suicide; RNA-seq, RNA sequencing; snRNA-seq, single-nucleus RNA sequencing; GPL570, Affymetrix Human Genome U133 Plus 2.0 platform.

2.3. Preprocessing, network construction and module testing

Discovery preprocessing and quality control. The normalized GSE101521 count matrix was mapped from Ensembl GRCh37.75 identifiers to gene symbols. Expression was transformed as log2(x+1). Genes were retained after an expression filter, reducing 62,069 input features to 34,006 expressed genes. The 5,000 genes with the highest median absolute deviation (MAD) were selected for network construction. Selecting high-MAD genes concentrates the analysis on reliably varying transcripts and limits computational noise, but it also defines the scope of the resulting network; low-variability genes cannot enter a module or become a hub.

Age, sex, RNA integrity number (RIN), post-mortem interval (PMI), and brain pH were treated as potential confounders or technical determinants of expression. Two RIN values and one PMI value were missing. The primary analysis replaced each missing value with the cohort median and included a corresponding missingness indicator, preserving all donors while allowing the model intercept to differ for imputed observations. A complete-case model assessed sensitivity to that decision. Principal-component analysis was used to inspect global sample structure and possible outliers; no sample was excluded solely because of its position in the first principal components; exclusion required a documented analytical reason rather than visual extremity.

Expression used to estimate the network was residualized for the covariates listed above. This step was intended to reduce correlation driven by age, sex, tissue quality, post-mortem interval, or pH rather than coordinated biology. Residualization cannot remove unmeasured influences such as detailed agonal factors, medication history, smoking, substance exposure, inflammatory illness, cortical layer sampling, or toxicology. Consequently, adjusted modules remain observational summaries rather than causal networks.

Weighted gene co-expression network analysis. A signed weighted gene co-expression network analysis (WGCNA) network was built from the residualized

5,000-gene matrix using biweight midcorrelation, which is less sensitive than Pearson correlation to isolated extreme values.[33] The soft-threshold power was selected by considering signed scale-free topology fit and mean connectivity. Power 8 produced a scale-free fit R^2 of 0.825 while retaining mean connectivity of 42.8. Adjacency values were transformed into topological overlap, genes were hierarchically clustered, and modules were defined with minimum module size 30, deepSplit 2, and merge cut height 0.25. Genes not assigned to a coherent module were labeled grey and were not interpreted as a biological module.

For each non-grey module, the first principal component of its standardized expression matrix was the module eigengene. Module membership (kME), the correlation between each gene and its module eigengene, ranked intramodular hubs, and the leading 300 genes by absolute kME were used for pathway analysis to provide a comparable annotation set across modules of different sizes, and network edges and hub ranks describe covariance in the discovery samples; they do not establish physical protein interaction, transcription-factor binding, directionality, or causal influence.

Module association models and multiplicity. Module eigengenes calculated on standardized original-scale expression were analyzed with empirical-Bayes linear models. Each model adjusted for age, sex, RIN, PMI, brain pH, and the RIN and PMI missingness indicators. The MDD-versus-control contrast combined MDD-S and MDD-NS and constituted the primary contrast. The three secondary contrasts retained the source phenotype distinctions. Coefficients are reported in standardized eigengene units, enabling comparison of direction and approximate magnitude across modules, but they should not be interpreted as gene-level fold changes.

Benjamini-Hochberg (BH) FDR correction was applied separately to the seven tested eigengenes, including grey as a technical comparator, within each contrast family. The inferential threshold was FDR < 0.05. This family structure answers whether any eigengene within a specified clinical contrast showed evidence after accounting for the number of tested eigengenes. Nominal p values are presented because they guided exploratory prioritization. However, they do not override the FDR result. No post hoc subset was used to claim statistical significance.

2.4. Functional annotation and cell-type composition

Functional and cell-marker enrichment. The top 300 genes by absolute kME in each module were submitted to g:Profiler for Gene Ontology Biological Process and Reactome enrichment, and enrichment identifies over-representation of an annotated gene set relative to a background; it does not show that the pathway is activated, inhibited, or phenotypically different. Directional statements were therefore based on eigengene coefficients rather than pathway labels.

Cell-marker enrichment used seven broad classes represented in GSE144136: excitatory neurons, inhibitory neurons, astrocytes, oligodendrocytes, OPCs, microglia/macrophages, and endothelial cells. Marker overlap was tested hypergeometrically using genes jointly measurable in the bulk network and reference as the universe. This universe prevents genes absent from one assay from inflating the apparent denominator. FDR correction was applied across the module-by-cell-type enrichment family. A large odds ratio indicates specificity of module membership to a marker list, not a change in cell abundance.

Control-derived reference and bulk deconvolution. The snRNA-seq reference was constructed from control nuclei only. The available control nuclei included 18,555 excitatory neurons, 6,422 inhibitory neurons, 2,632 astrocytes, 3,200 oligodendrocytes, 1,157 OPCs, 542 microglia/macrophages, and 192 endothelial cells. Unequal nucleus counts can affect signature precision, especially for rarer populations. Reference expression was derived without incorporating MDD-S nuclei so that a disease-associated expression change would not be built into the reference profile and then mistaken for a compositional shift.

After intersecting reference markers with the bulk matrix, 509 markers entered constrained quadratic programming. Estimated coefficients were required to be non-negative and sum to one. Marker bootstrap resampling with 100 replicates characterized numerical uncertainty. Because fractions are compositional, inferential models used centered log-ratio (CLR) transformations. For a D-part composition x, $\mathrm{CLR}(x_i) = \ln[x_i/g(x)]$, where $g(x) = (\prod_{j=1}^{D} x_j)^{1/D}$. A CLR coefficient therefore expresses change in one component relative to the geometric mean of all components; it is not an absolute percentage-point difference and cannot identify whether one cell population changed independently of the rest.

Two populations, inhibitory neurons and OPCs, were below the numerical identifiability threshold in the bulk deconvolution and were not tested inferentially; excluding these unstable estimates prevents near-zero coefficients from being reported with spurious precision, and the five estimable populations were tested in adjusted MDD-versus-control models and corrected by BH-FDR. Bulk fractions were interpreted as relative transcriptomic contributions rather than direct stereological counts.

Direct donor-level snRNA-seq composition. For the direct GSE144136 analysis, annotated nuclei were counted within each donor and divided by that donor's total classified nuclei to obtain seven proportions. Statistical models were fitted to donor-level CLR values and adjusted for batch. This preserves the human donor as the unit of replication and avoids pseudoreplication that would occur if tens of thousands of nuclei were treated as independent case-control observations. BH-FDR correction was applied across the seven cell types.

Raw mean proportions are reported for descriptive accessibility, whereas inferential conclusions follow the

CLR models. An increase in the CLR of a population means that its proportion increased relative to the geometric mean composition. Accordingly, a positive neuronal coefficient can occur even when its raw mean percentage changes only slightly, if other components decline more strongly, and observed nuclear composition may represent biology, differential nuclear recovery, tissue sampling, annotation, or combinations of these mechanisms; the analysis does not equate it with absolute cell number.

2.5. External validation and sensitivity analyses

External validation. GSE54568 microarray probes were mapped to gene symbols, and the probe with the greatest MAD was retained when several probes represented one gene. Each discovery module score was calculated with its discovery kME values as locked weights. This procedure asks whether the coordinated direction learned in RNA sequencing transfers to an independent platform and cohort. It is more conservative than reconstructing modules in the validation data, which would assess a newly optimized network rather than reproduce the discovery signal.

Within each of 15 matched pairs, the control score was subtracted from the MDD score. Paired differences, 95% confidence intervals, and FDR values were calculated for testable modules. The red module was not tested because too few mapped genes met the gene-mapping threshold. Directional concordance compared the sign of discovery and validation effects. Edge preservation was summarized as the correlation between within-module gene-pair correlations in discovery and validation. Replication required more than a positive edge correlation: the phenotype-score association also needed a compatible direction and uncertainty that supported a non-zero difference.

Sensitivity analyses and analytical checks. The primary MDD-versus-control module models were repeated in complete cases and after excluding the seven donors younger than 18 years. These analyses assessed whether imputation or the broad age range accounted for the main module pattern. They were not treated as additional opportunities for significance and were interpreted by direction, magnitude, and FDR.

Cross-file checks verified that module sizes summed to 5,000 genes, network identifiers were unique, FDR calculations corresponded to their contrast families, cell fractions and observed proportions were bounded and summed to one within tolerance, and donor and mapped-gene counts agreed across outputs.

2.6. Ethical approval

Ethical approval was granted by the CMHC Research Center Ethics Committee Indonesia (No. 2026/0190). The study used publicly available, de-identified post-mortem datasets; consent and tissue donation were governed by the original source studies.

3. Results

3.1. Discovery cohort and network structure

The discovery analysis included all 59 donors. The MDD-NS subgroup was the smallest (n = 9), and estimates involving that subgroup consequently had wider sampling uncertainty than the overall MDD-versus-control contrast. Tissue-quality measures were broadly within ranges compatible with transcriptomic analysis, although MDD-S donors had a lower median RIN and a longer mean PMI than controls. These variables, along with age, sex, and brain pH, were included in the adjusted models rather than used as exclusion criteria.

At power 8, the signed network assigned genes to six non-grey modules: turquoise (592 genes), blue (541), brown (509), yellow (242), green (225), and red (75). The remaining genes were grey. The modules differed in biological interpretability. Turquoise was led by GLDN and annotated by axon ensheathment and myelination; brown was led by EMP1 and annotated by inflammatory and immune responses. Other leading annotations included regulation of glucagon secretion in yellow, olfactory-receptor-related expression in green, and intestinal saccharidase-related terms in red. The latter annotations were driven by available gene-set labels and were not assumed to represent literal intestinal physiology in DLPFC tissue.

The complete adjusted module-trait pattern is shown in Figure 1. No single module had a uniformly large association across all phenotype contrasts. The visually strongest negative estimates involved brown in MDD contrasts and blue in the MDD-S versus MDD-NS contrast. The pattern supports selective exploratory hypotheses rather than a global separation of diagnostic groups by the co-expression network.

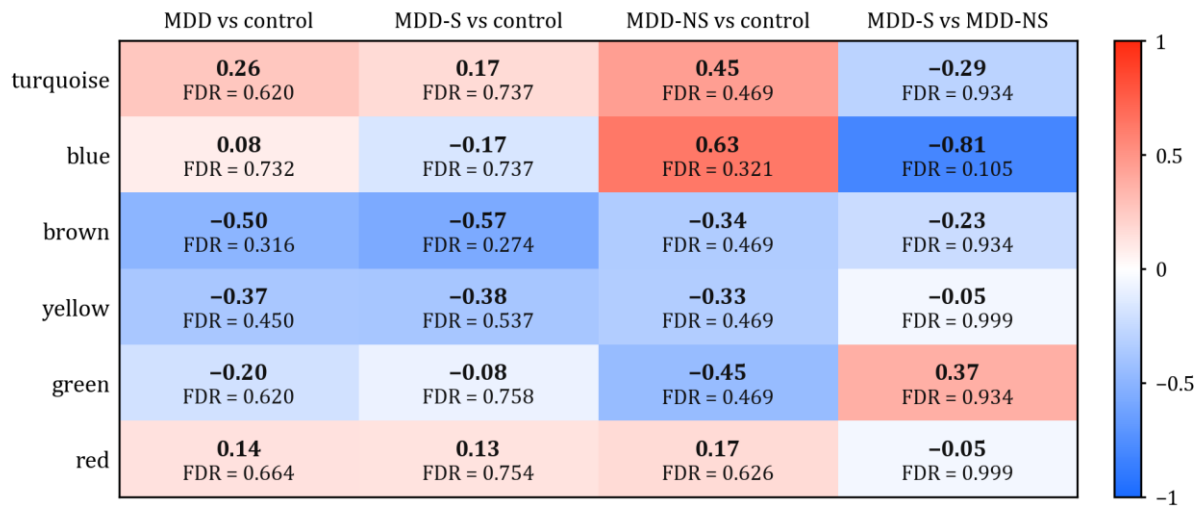


Figure 1. Adjusted module-eigengene associations across phenotype contrasts. Columns are the contrasts MDD vs control, MDD-S vs control, MDD-NS vs control, and MDD-S vs MDD-NS; each cell gives the adjusted coefficient (standardized eigengene units) and its FDR. Color encodes coefficient direction and magnitude; displayed FDR values govern inference. No module reached FDR < 0.05.

3.2. Module eigengene associations

In the primary MDD-versus-control model, the brown eigengene was lower in MDD by 0.499 standardized units (p = 0.045), but its FDR was 0.316. Yellow was also lower (β = −0.366; p = 0.129; FDR = 0.450). Turquoise, despite strong oligodendrocyte annotation, was not associated with MDD (β = +0.256; FDR = 0.620). The absence of FDR < 0.05 means that no primary module association met the inferential threshold (FDR < 0.05).

For MDD-S versus control, brown again had the largest prioritized signal (β = −0.570; p = 0.039; FDR = 0.274), followed by yellow (β = −0.382; p = 0.153; FDR = 0.537). This repeated negative direction makes brown a coherent within-discovery candidate, but the evidence remains nominal and correlated across contrasts because MDD-S contributes to the combined MDD group. It is not two independent replications.

For MDD-NS versus control, blue was higher by 0.633 standardized units (p = 0.046; FDR = 0.321), while turquoise was higher by 0.454 units (p = 0.183; FDR = 0.469). For MDD-S versus MDD-NS, blue showed the largest coefficient in the entire contrast set (β = −0.807; p = 0.015; FDR = 0.105). Because only nine MDD-NS donors contributed to these comparisons, the coefficient is compatible with a potentially meaningful subgroup difference but is also susceptible to sampling variability and magnitude inflation. Module architecture and the leading adjusted contrasts are detailed in Table 2 without converting nominal results into confirmatory claims.

Table 2. Co-expression module architecture and leading adjusted phenotype estimates.

Module	Genes	Leading hub / annotation	Leading contrast	β (p)	FDR
Turquoise	592	GLDN / axon ensheathment	MDD vs control	+0.256	0.620
Blue	541	MUC5B / GALNT12-related set	MDD-S vs MDD-NS	-0.807 (0.015)	0.105
Brown	509	EMP1 / inflammatory response	MDD vs control	-0.499 (0.045)	0.316
Brown	509	EMP1 / inflammatory response	MDD-S vs control	-0.570 (0.039)	0.274
Yellow	242	RP11-381O7.3 / glucagon-regulation set	MDD vs control	-0.366 (0.129)	0.450
Green	225	RP11-309H21.3 / olfactory-receptor set	MDD-S vs MDD-NS	+0.366 (0.316)	0.934
Red	75	RP11-782C8.5 / saccharidase-related set	MDD vs control	+0.140	0.664

Notes: β values are adjusted differences in standardized eigengene units. Benjamini-Hochberg FDR was calculated within each seven-eigengene contrast family. No module reached FDR < 0.05. MDD, major depressive disorder; MDD-NS, MDD who died from other causes; MDD-S, MDD who died by suicide; FDR, false-discovery rate; hub, gene with the highest module membership (kME) in the module.

3.3. Brown inflammatory module

The brown module contained 509 genes. Its highest module-membership values included EMP1 (kME = 0.85), ZFP36 (0.85), SOCS3 (0.81), TNFRSF12A (0.81), CD93 (0.80), TNFRSF10A (0.80), IL8 (0.80), SERPINE1 (0.80), GPRC5A (0.79), MT1A (0.77), HSPA7 (0.77), and GPR97 (0.77). These genes span immediate-response regulation, cytokine signaling, endothelial or vascular biology, stress responses, and myeloid-associated processes. The strongest functional label was inflammatory response (g:Profiler FDR = 3.77 × 10^{-20}),

accompanied by immune-system process, defense response, and leukocyte migration.

This enrichment shows internally coherent inflammatory biology in the discovery network. It does not mean that inflammation was significantly lower in MDD, because the pathway test and phenotype test address different questions. The module-level coefficient indicates that the weighted expression pattern tended to be lower in MDD, especially MDD-S, but the adjusted association did not survive module-family correction. Furthermore, the external score changed in the opposite direction. The most defensible inference is therefore that a reproducible inflammatory module was identifiable as a structure within GSE101521, whereas its relationship to MDD status remains uncertain.

3.4. Turquoise oligodendrocyte-related module

The 592-gene turquoise module was led by GLDN and enriched for myelination, axon ensheathment, and oligodendrocyte differentiation. Among 284 module genes measurable in the shared network-reference universe, 37 were oligodendrocyte markers, yielding an odds ratio of 520.45 and FDR of 2.14×10^{-31}. This was the only module-by-cell-type enrichment to remain significant after correction and provides strong evidence that the network recovered a canonical cell-associated transcriptional program.

The eigengene itself was not associated with MDD (β = +0.256; FDR = 0.620). This contrast is informative: a module can have highly specific cell identity and still show no case-control difference. The finding supports the technical and biological face validity of the network while arguing against an overall shift in the turquoise program in this sample. It also cautions against using enrichment strength as a surrogate for phenotype effect size.

3.5. Bulk-deconvolved composition

Among the five estimable bulk components, the largest MDD-versus-control CLR coefficient was observed for astrocytes (β = −0.644; p = 0.085; FDR = 0.598). Oligodendrocytes (β = +0.507; p = 0.386; FDR = 0.748), microglia/macrophages (β = +0.281; p = 0.462; FDR = 0.748), endothelial cells (β = +0.222; p = 0.526; FDR = 0.748), and excitatory neurons (β = −0.120; p = 0.805; FDR = 0.805) showed no multiplicity-adjusted association. No bulk fraction reached FDR < 0.05.

The astrocyte direction is compatible with the direct snRNA-seq composition result, but it does not constitute replication: the assays, samples, phenotype contrasts, and estimands differ. Bulk deconvolution estimates relative transcriptomic contributions using transferred marker profiles, whereas direct snRNA-seq counts recovered and classified nuclei. The lack of a corrected bulk association may reflect limited power, cross-assay signature transfer, unmodeled cell states, or genuinely small composition differences. It also indicates that the nominal brown signal cannot be reduced to a demonstrated bulk astrocyte proportion change.

3.6. Direct donor-level cell composition

In GSE144136, astrocytes accounted for a mean 9.2% of classified nuclei in controls and 3.4% in MDD-S. The adjusted donor-level CLR coefficient was −1.264 (FDR = 0.002). Excitatory neurons increased descriptively from 55.3% to 63.5% (β = +0.691; FDR = 0.024). Inhibitory neurons had similar raw means, 20.5% and 20.9%, yet a positive CLR coefficient (β = +0.489; FDR = 0.024) because their relative position increased against the geometric mean of the full composition.

Microglia/macrophages averaged 1.6% in controls and 2.1% in MDD-S (βCLR = +0.444; FDR = 0.215). Oligodendrocytes, OPCs, and endothelial cells had negative CLR estimates with FDR = 0.589. Donor-level CLR estimates and their 95% confidence intervals are shown in Figure 2. Thus, the clearest multiplicity-adjusted evidence in the study came from relative astrocyte, excitatory-neuron, and inhibitory-neuron composition in this male MDD-S dataset. These results describe the recovered nuclear pool and do not demonstrate astrocyte loss, neuronal proliferation, or a diagnosis-specific mechanism.

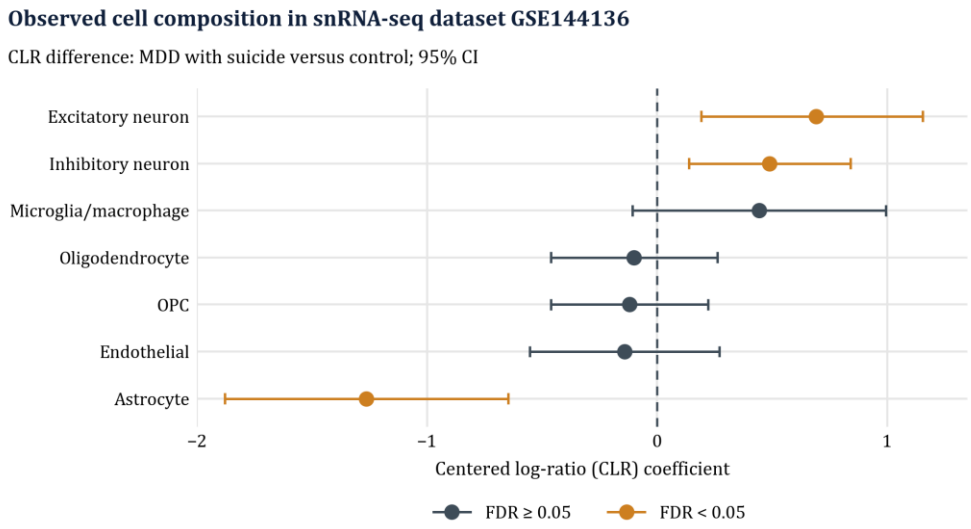


Figure 2. Donor-level centered log-ratio differences in observed GSE144136 cell composition. Points are adjusted coefficients and bars are 95% confidence intervals; gold denotes FDR < 0.05. Effects are relative compositional differences, not absolute cell counts. All donors were male.

3.7. External validation

Five modules met the gene-mapping threshold in GSE54568. The yellow score difference was +0.204 (95% CI −0.090 to +0.499; FDR = 0.791), turquoise was −0.120 (−0.440 to +0.200; FDR = 0.888), brown was +0.081 (−0.191 to +0.354; FDR = 0.888), green was −0.049 (−0.377 to +0.279; FDR = 0.941), and blue was +0.008 (−0.353 to +0.370; FDR = 0.961). External paired module-score estimates and their 95% confidence intervals are shown in Figure 3. Every interval crossed zero, and no module met FDR < 0.05.

Only blue and green showed the same score direction as their relevant discovery MDD contrast. Brown, the leading discovery candidate, reversed direction. Edge-correlation coefficients were 0.127 for yellow, 0.176 for turquoise, 0.274 for brown, 0.101 for green, and −0.007 for blue. The modest positive brown edge correlation suggests that some internal covariance persisted across platforms, but the phenotype-associated score did not reproduce. Structural similarity without a concordant phenotype difference was not considered replication.

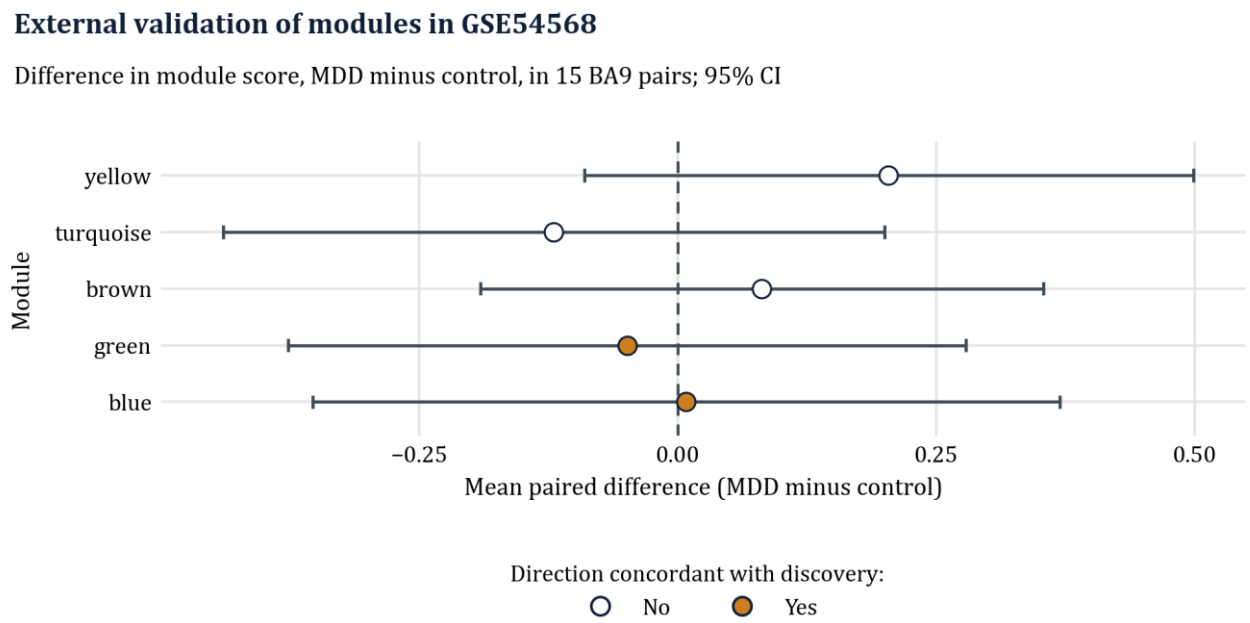


Figure 3. External evaluation of discovery-weighted module scores in 15 matched GSE54568 pairs. Points are paired MDD-minus-control differences and bars are 95% confidence intervals. Every interval crossed zero and every FDR exceeded 0.05. Filled points mark modules whose score difference had the same direction as the relevant discovery MDD contrast; open points mark the opposite direction.

3.8. Sensitivity analyses

In the primary analysis, the brown MDD-versus-control coefficient was −0.499 with FDR = 0.316. It remained negative in complete cases (β = −0.439; FDR = 0.496) and among donors aged at least 18 years (β = −0.598; FDR = 0.221). Turquoise remained positive across the primary (+0.256), complete-case (+0.224), and adult-only (+0.337) models, with FDR values of 0.620, 0.518, and 0.508. Yellow, green, and the remaining modules likewise showed broadly stable directions, but no sensitivity estimate reached FDR < 0.05.

The sensitivity results reduce concern that median-plus-indicator handling or the inclusion of younger donors solely produced the brown direction. They do not resolve the external reversal or create confirmatory evidence. Composition, validation, and sensitivity estimates are detailed in Table 3 so that robustness within discovery can be considered alongside failure of cross-cohort phenotype replication.

Table 3. Cell-composition, external-validation, and sensitivity findings.

Analysis	Item	Estimate	FDR / interpretation
Bulk deconvolution	Astrocyte	βCLR = −0.644; p = 0.085	FDR = 0.598; no bulk cell component significant
Direct snRNA-seq	Astrocyte	9.2% (control) vs 3.4% (MDD-S); βCLR = −1.264	FDR = 0.002
Direct snRNA-seq	Excitatory neuron	55.3% (control) vs 63.5% (MDD-S); βCLR = +0.691	FDR = 0.024
Direct snRNA-seq	Inhibitory neuron	20.5% (control) vs 20.9% (MDD-S); βCLR = +0.489	FDR = 0.024; relative CLR effect
External validation	Brown module	Δ = +0.081 (95% CI −0.191 to +0.354)	FDR = 0.888; direction reversed
External validation	Blue module	Δ = +0.008 (95% CI −0.353 to +0.370)	FDR = 0.961; direction concordant
Sensitivity	Brown, complete cases	β = −0.439	FDR = 0.496; negative direction retained
Sensitivity	Brown, age ≥18 years	β = −0.598	FDR = 0.221; negative direction retained

Notes: Cell percentages are descriptive donor means. CLR coefficients represent change relative to the geometric mean composition. External Δ is paired MDD minus control. No module replicated externally. CI, confidence interval; FDR, false-discovery rate; MDD, major depressive disorder; MDD-S, MDD who died by suicide; snRNA-seq, single-nucleus RNA sequencing.

4. Discussion

4.1. Principal findings

The study separated four layers of evidence in post-mortem DLPFC transcriptomics. First, WGCNA found biologically coherent co-expression architecture, above all an inflammatory brown module and an oligodendrocyte-related turquoise module. Second, no module eigengene was associated with MDD or with the suicide-related contrasts after FDR correction. Brown and blue stood out on nominal evidence alone. Third, direct donor-level snRNA-seq composition showed corrected relative differences in astrocytes and neuronal populations, which bulk deconvolution did not. Fourth, discovery-weighted module scores failed to replicate in an independent paired microarray cohort. The results thus back specific, cell-contextualized hypotheses. They do not back a stable DLPFC module biomarker for MDD or suicide.

Module annotation and phenotype association must be kept apart. The turquoise module is extremely enriched for oligodendrocyte markers, so WGCNA clearly recovered a recognizable biological program. Yet its eigengene was not associated with disease, which shows that cell specificity alone does not imply disease alteration. The brown module works the same way. Its inflammatory enrichment is no proof that inflammatory activity was lower in MDD. Its within-discovery coefficients were negative, but the FDR values exceeded 0.05 and the external score reversed direction. Reading the layers separately stops a strong functional label from lending false certainty to an uncertain case-control effect.

4.2. Comparison with the existing literature

Immune-glial co-expression in context. The brown module broadly matches the immune, glial, chemokine, endothelial, and vascular findings of the original GSE101521 report.[1] Among its hubs, ZFP36 and SOCS3 take part in feedback control of inflammatory signaling. IL8 and SERPINE1 can mark inflammatory and vascular responses. CD93 and TNFRSF12A link to endothelial or tissue-remodeling biology. The module looks like a composite immune-glial-vascular entity, not a single cell type or pathway.

Post-mortem transcriptomic studies have repeatedly implicated immune and glial mechanisms in subsets of depression and suicide, yet the direction of change varies,[3–7,10,15–18,21,24,25,29,30] and acute inflammation, metabolic disease, smoking, medication, cause and method of death, agonal interval, tissue pH, and cell representation can each shift immune-associated RNA. A lower brown eigengene might mean reduced expression within the relevant cells. It might equally mean fewer contributing cells, altered cellular states, or residual confounding. The deconvolved bulk astrocyte estimate was negative but not significant, and microglial composition did not change after correction. The present data therefore cannot attribute the module difference to any one population.

The external reversal matters. It argues against reading the brown pattern as a general direction of MDD biology. The validation cohort used another platform, contained matched pairs, and did not mirror the discovery phenotype structure exactly. Platform attenuation and mapping loss may weaken a score, but they give no licence to ignore its direction. A confirmation study should measure a locked panel of brown hub genes, by RNA sequencing or targeted assays, in an equivalently phenotyped four-group cohort. Agreement in eigengene direction, key hubs, and orthogonal cell-state measures would persuade more than pathway enrichment alone.

Oligodendrocyte and myelination architecture. The turquoise module offers a counterpoint. Its enrichment for oligodendrocyte markers and myelination-related processes was striking and fits the central role of oligodendrocyte-lineage transcription in cortical tissue covariance. Single-nucleus work in MDD DLPFC has pointed to OPCs and deep-layer excitatory neurons as sites of extensive differential expression.[2,13,26,27,31,32] Cross-region and cross-disorder analyses likewise identify glial and myelination programs as recurrent but

heterogeneous parts of psychiatric transcriptomics.[1,4,6,16,27,31]

Here, neither the turquoise eigengene nor bulk oligodendrocyte composition differed after correction, and direct GSE144136 oligodendrocyte and OPC proportions were also non-significant. None of this contradicts cell-type-specific differential expression inside oligodendrocytes or OPCs. A stable relative abundance can sit alongside extensive within-cell transcriptional change. A marker-enriched bulk module, conversely, may track the presence of a lineage and miss a disease-relevant state. Settling the question calls for cell-type-specific expression analysis or spatially resolved measurement. Bulk enrichment cannot do it.

Relative astrocyte and neuronal composition. The strongest corrected results were the donor-level compositional differences in GSE144136. The mean recovered astrocyte proportion was lower in MDD-S, and the excitatory and inhibitory neuronal CLR values were higher. Astrocytes regulate glutamate uptake, metabolic support, extracellular ion balance, synaptic maintenance, and neurovascular coupling. A lower relative astrocyte signal is therefore relevant to hypotheses of altered cortical homeostasis in depression. It cannot, however, establish astrocyte loss or dysfunction. Cell types differ in nuclear recovery, astrocyte nuclei may be more vulnerable to tissue handling, and proportions always move relative to one another.

The inhibitory-neuron result shows why raw percentages and CLR coefficients need to be read together. Mean proportions of inhibitory neurons were almost identical across groups, yet the CLR coefficient was positive because other components changed. The result is valid for relative composition. It should not be narrated as a large absolute rise in inhibitory neurons. The higher excitatory-neuron proportion is open to several readings: better recovery of neuronal nuclei, poorer recovery of astrocytes, cortical-layer sampling, or a true biological shift, and quantitative histology, stereology, nuclei-recovery experiments, and spatial transcriptomics would be needed to tell them apart.

The GSE144136 design also limits attribution. Every case had MDD and died by suicide. Controls shared neither characteristic. All donors were male. The observed composition could therefore relate to MDD, to suicide, to their interaction, to male-specific biology, or to correlated clinical and technical features. Sex- and symptom-resolved human studies show marked molecular heterogeneity, so extrapolating to women would be especially unwarranted.[14,17] Isolating these dimensions would take a factorial design with controls who died from non-suicide causes, psychiatric or non-psychiatric suicide controls, MDD-NS, and MDD-S, in both sexes.

Bulk deconvolution versus direct composition. Bulk deconvolution and direct nuclear composition diverge, and the divergence is more than a clash between a negative and a positive test. The two analyses estimate different quantities. Bulk deconvolution uses a reference to allocate mixed-tissue RNA to idealized cell classes, so its coefficients may reflect cell abundance, RNA content per cell, cell state, marker specificity, and assay compatibility. Direct snRNA-seq composition counts recovered nuclei assigned to clusters. That is closer to the sampled cellular mixture, but isolation and annotation still influence it. Neither quantity is an unbiased absolute cell count.

The astrocyte estimates pointed the same way in both approaches, which helps to prioritize hypotheses. Formal replication, though, would require equivalent phenotypes and estimands. The discovery cohort merged MDD-S and MDD-NS for the primary contrast and included both sexes. GSE144136 compared male MDD-S with male controls. Using the direct result to declare the non-significant bulk estimate significant after the fact would mislead. What the shared direction does is single out astrocyte representation as a targeted question for an independent assay specified in advance.

Bulk deconvolution also could not estimate inhibitory neurons and OPCs reliably. This shows a practical limit of broad-cell-class deconvolution, since closely related neuronal signatures and low or overlapping marker contributions create identifiability problems. Reporting these populations as zero would mix up numerical non-identifiability and biological absence. Leaving them out of inference, and adding marker bootstrap uncertainty and CLR modeling, gives a more defensible analysis, even though fewer cell types can be compared directly.

4.3. Interpretation and mechanism

Suicide-related contrasts. The blue module gave the largest MDD-S versus MDD-NS estimate, with an FDR of 0.105 and only nine MDD-NS donors. It was also nominally higher in MDD-NS versus control. The suicide contrast may thus partly reflect a rise in the small non-suicide group, not a selective fall in MDD-S. Without a non-MDD suicide group, suicide cannot be separated from diagnosis. A large coefficient picked out of several modules and contrasts may also be inflated by sampling variability, the winner's curse.

Larger post-mortem studies show that the molecular correlates of completed suicide depend on the comparison group, the method, and the psychiatric diagnosis.[3,7,15,16,21,23–25,29] DLPFC network findings involving mitochondrial, purinergic, synaptic, or cytokine pathways may be genuine in particular biological subgroups and still fail to generalize across all suicides. The blue result should be treated as an exploratory contrast. Testing it needs a design with adequate MDD-NS representation and a suicide control group. It must not be read as a molecular risk score or as a marker of suicidal intent in living patients.

External validation and reproducibility. No module met the external phenotype-replication criterion. This negative result carries more weight than the visual appeal of an enriched discovery module. Validation applied discovery kME weights instead of relearning modules, kept the matched-pair structure, and reported confidence intervals, FDR, direction, and edge correlation. These choices pose a stringent question:

does the same weighted transcriptional program differ in an independent cohort? For brown, the answer was no, despite a modestly positive edge correlation.

Validation across platforms is hard. Microarrays have restricted probe coverage and dynamic range. Picking one probe per gene discards transcript-level complexity. Only some module genes mapped. The clinical composition of GSE54568 did not reproduce every discovery contrast. All of this widens uncertainty and can attenuate effects. It is a reason to look for a better matched validation cohort. It is not a reason to relabel the present result as a success. A module meant for broad biological or clinical interpretation has to tolerate at least some reasonable variation in platform and sampling.

Several modules showed small positive edge correlations, which suggests partial conservation of covariance structure. Network preservation and phenotype replication nonetheless answer different questions. A stable oligodendrocyte program may be present in every human DLPFC sample without differing by MDD. Equally, a phenotype-associated score could emerge even if fine-grained edge structure changes, and future studies should state which property they aim to reproduce and report both when they claim a replicated network finding.

4.4. Implications for research and practice

Statistical and practical importance. Statistical and biological importance should not be collapsed, and this study shows why. The brown and blue coefficients were moderate in standardized units, and the brown module had highly significant functional enrichment. Multiplicity-adjusted uncertainty and external non-replication still rule out the conclusion that these modules characterize MDD in general. The astrocyte CLR result was statistically robust within GSE144136, but the absolute and clinical meaning of a relative nuclear-composition shift remains unclear. None of these post-mortem quantities has been tied to symptoms, treatment response, prospective suicide risk, or diagnostic discrimination.

The findings therefore give no support to clinical testing, patient stratification, or risk prediction. Their practical value lies in narrowing experimental questions. The brown hubs form a tractable immune-glial-vascular panel. The astrocyte result suggests a target for spatial or histological quantification, and the blue contrast defines a network hypothesis for better balanced suicide designs; that is a meaningful contribution, provided it is presented as prioritization and not as premature translation.

Implications for future research. A decisive follow-up should recruit or pool enough post-mortem samples for a factorial design that separates psychiatric diagnosis from suicide status. At minimum it needs non-psychiatric non-suicide controls, suicide donors without MDD where ethics and diagnosis allow, MDD-NS donors, and MDD-S donors. Both sexes should be represented, and key agonal and toxicological variables harmonized. The analysis plan should name one primary contrast and a small number of locked modules before outcome data are inspected.

Replication should keep the discovery gene set and weights, or test a targeted panel defined in advance. RNA sequencing across cohorts would cut cross-platform mapping loss. Targeted digital expression assays could confirm brown hubs efficiently. Spatial transcriptomics, single-nucleus multiome profiling, and quantitative immunohistochemistry could separate altered abundance from altered state and place immune-glial signals in cortical layers or vascular niches, and absolute cell-count methods matter most for interpreting relative astrocyte and neuronal composition.

Later work should also ask whether molecular patterns map onto clinically interpretable dimensions, not diagnosis alone, while avoiding circular subgroup selection, and symptom severity, psychotic features, chronicity, medication exposure, inflammatory comorbidity, and suicide method may define biologically relevant strata. Each needs adequate sample size and independent confirmation. The present findings supply hypotheses and effect-direction information for such designs. They supply no validated clinical thresholds.

4.5. Strengths and limitations

Strengths. Several design features add strength. The three datasets had explicit, non-overlapping analytical roles. The discovery cohort kept MDD-S and MDD-NS as separate categories, so suicide status was not merged out of sight. Network construction adjusted expression for the main tissue and demographic covariates, and the phenotype models included those covariates again at the eigengene level. The cell reference came from controls only, which limited disease leakage into deconvolution. Direct nuclear composition was analyzed at donor level, not by treating nuclei as independent observations. Multiple-testing correction was kept for each outcome family, and sensitivity analyses addressed missing covariates and younger donors.

The external analysis was also built to be falsifiable. Discovery weights were locked, gene-mapping loss was reported, matched pairs were respected, and non-replication was stated openly. The interpretation, finally, separates internal biological coherence, phenotype association, composition, and external validation. In high-dimensional studies this separation matters most, because a strongly enriched pathway can otherwise overshadow uncertain disease evidence.

Limitations. Sample size is the main limitation, and especially the nine MDD-NS donors. A network built on 59 samples can find broad modules but estimates subtle module-trait effects and subgroup interactions imprecisely. Multiple-testing correction rightly reflects this uncertainty. The discovery cohort also spans a wide age range and includes seven donors younger than 18 years. Adult-only estimates pointed the same way. The developmental breadth still matters, because cortical

cell composition and transcription change across the lifespan.

Statistical adjustment cannot remove post-mortem confounding. PMI, pH, and RIN were modeled. Detailed agonal state, systemic illness, medication exposure, smoking, substance use, toxicology, circadian timing, and tissue dissection may remain. Cause of death is tied intrinsically to the MDD-S group. Residualizing expression before network construction lowers the influence of measured covariates. It may also alter genuine covariate-associated biology, and it cannot correct unmeasured factors.

The deconvolution reference and the bulk assay differ in measurement scale, RNA capture, and cellular representation. Broad cell classes hide heterogeneous states and cortical layers. Two cell types were not identifiable in bulk. The 100 marker bootstraps describe the stability of marker selection, not every source of uncertainty, and direct snRNA-seq composition is male-only and confounds MDD with suicide. It also reflects recovered nuclei, not absolute tissue counts.

External validation used a microarray cohort with incomplete module-gene coverage and non-equivalent phenotype detail. The red module could not be tested. The 15 pairs left confidence intervals wide, and failure to replicate therefore does not prove that all related biology is absent, and it does mean that the specific discovery-weighted phenotype effects were not shown in the external cohort available. Finally, the analysis is observational and cross-sectional. It cannot show whether transcriptomic or compositional differences preceded MDD, followed from illness or treatment, reflected the terminal event, or were compensatory.

5. Conclusion

Covariate-adjusted WGCNA of GSE101521 identified six DLPFC co-expression modules, including an inflammatory brown module and an oligodendrocyte-related turquoise module, but no eigengene association survived FDR correction (brown was nominally lower in MDD and MDD-S, and blue showed the largest MDD-S versus MDD-NS estimate), and bulk deconvolution likewise showed no corrected cell-fraction difference. Direct donor-level GSE144136 composition showed lower relative astrocyte and higher relative neuronal representation in male MDD-S, which cannot separate diagnosis, suicide, sex, and nuclear recovery, and discovery-weighted module scores did not replicate in GSE54568. The study therefore prioritizes immune-glial, astrocytic, and neuronal hypotheses for rigorously matched, cell-resolved replication. It gives no basis for diagnostic or suicide-risk biomarker use.

Declarations

Use of Generative Artificial Intelligence. None declared.

Author Contributions. A.H.: conceptualization, methodology, software, formal analysis, investigation, data curation, visualization, writing – original draft. J.W.: validation, supervision, writing – review & editing. Both authors approved the final manuscript.

Funding. This research received no specific funding.

Conflict of Interest. The authors declare that they have no competing interests.

Ethical Approval. Ethical approval was granted by the CMHC Research Center Ethics Committee Indonesia (No. 2026/0190).

Informed Consent. Informed consent was not applicable to this secondary analysis of public, de-identified datasets. Consent and tissue-donation procedures were governed by the original source studies.

Data Availability. The datasets analyzed are publicly available from the NCBI Gene Expression Omnibus under accession numbers GSE101521, GSE144136, and GSE54568. No new participant-level data were generated.

Acknowledgements. None.

References

1. Pantazatos SP, Huang YY, Rosoklija GB, et al. Whole-transcriptome brain expression and exon-usage profiling in major depression and suicide: evidence for altered glial, endothelial and ATPase activity. Mol Psychiatry. 2017;22(5):760-773. doi:10.1038/mp.2016.130
2. Nagy C, Maitra M, Tanti A, et al. Single-nucleus transcriptomics of the prefrontal cortex in major depressive disorder implicates oligodendrocyte precursor cells and excitatory neurons. Nat Neurosci. 2020;23(6):771-781. doi:10.1038/s41593-020-0621-y
3. Punzi G, Ursini G, Chen Q, et al. Genetics and brain transcriptomics of completed suicide. Am J Psychiatry. 2022;179(3):226-241. doi:10.1176/appi.ajp.2021.21030299
4. Jaffe AE, Tao R, Page SC, et al. Decoding shared versus divergent transcriptomic signatures across cortico-amygdala circuitry in PTSD and depressive disorders. Am J Psychiatry. 2022;179(9):673-686. doi:10.1176/appi.ajp.21020162
5. Shukla R, Newton DF, Sumitomo A, et al. Molecular characterization of depression trait and state. Mol Psychiatry. 2022;27(2):1083-1094. doi:10.1038/s41380-021-01347-z
6. Chandley MJ, Szebeni A, Szebeni K, et al. Markers of elevated oxidative stress in oligodendrocytes captured from the brainstem and occipital cortex in major depressive disorder and suicide. Prog Neuropsychopharmacol Biol Psychiatry. 2022;117:110559. doi:10.1016/j.pnpbp.2022.110559
7. Dóra F, Renner É, Keller D, et al. Transcriptome profiling of the dorsomedial prefrontal cortex in suicide victims. Int J Mol Sci. 2022;23(13):7067. doi:10.3390/ijms23137067
8. Xia M, Liu J, Mechelli A, et al. Connectome gradient dysfunction in major depression and its association with gene expression profiles and treatment outcomes. Mol Psychiatry. 2022;27(3):1384-1393. doi:10.1038/s41380-022-01519-5
9. Zhao X, Logue MW, Hawn SE, et al. PTSD, major depression, and advanced transcriptomic age in brain tissue. Depress Anxiety. 2022;39(12):824-834. doi:10.1002/da.23289
10. Chen Y, Dai J, Tang L, et al. Neuroimmune transcriptome changes in patient brains of psychiatric and neurological disorders. Mol Psychiatry. 2023;28(2):710-721. doi:10.1038/s41380-022-01854-7
11. Xue K, Guo L, Zhu W, et al. Transcriptional signatures of the cortical morphometric similarity network gradient in first-episode, treatment-naive major depressive disorder.

Neuropsychopharmacology. 2023;48(3):518-528. doi:10.1038/s41386-022-01474-3

12. Liu S, Abdellaoui A, Verweij KJH, et al. Gene expression has distinct associations with brain structure and function in major depressive disorder. Adv Sci (Weinh). 2023;10(7):e2205486. doi:10.1002/advs.202205486
13. Chatzinakos C, Pernia CD, Morrison FG, et al. Single-nucleus transcriptome profiling of dorsolateral prefrontal cortex: mechanistic roles for neuronal gene expression, including the 17q21.31 locus, in PTSD stress response. Am J Psychiatry. 2023;180(10):739-754. doi:10.1176/appi.ajp.20220478
14. Mansouri S, Pessoni AM, Marroquín-Rivera A, et al. Transcriptional dissection of symptomatic profiles across the brain of men and women with depression. Nat Commun. 2023;14(1):6835. doi:10.1038/s41467-023-42686-5
15. Peng S, Zhou Y, Xiong L, et al. Identification of novel targets and pathways to distinguish suicide dependent or independent on depression diagnosis. Sci Rep. 2023;13(1):2488. doi:10.1038/s41598-023-29101-1
16. Zhou Y, Xiong L, Chen J, et al. Integrative analyses of scRNA-seq, bulk mRNA-seq, and DNA methylation profiling in depressed suicide brain tissues. Int J Neuropsychopharmacol. 2023;26(12):840-855. doi:10.1093/ijnp/pyad057
17. Brown SJ, Christofides K, Weissleder C, et al. Sex- and suicide-specific alterations in the kynurenine pathway in the anterior cingulate cortex in major depression. Neuropsychopharmacology. 2024;49(3):584-592. doi:10.1038/s41386-023-01736-8
18. Zhuang Q, Zhang R, Li X, et al. Identification of the shared molecular mechanisms between major depressive disorder and COVID-19 from postmortem brain transcriptome analysis. J Affect Disord. 2024;346:273-284. doi:10.1016/j.jad.2023.11.030
19. Arakelyan A, Avagyan S, Kurnosov A, et al. Temporal changes of gene expression in health, schizophrenia, bipolar disorder, and major depressive disorder. Schizophrenia (Heidelb). 2024;10(1):19. doi:10.1038/s41537-024-00443-7
20. Liu W, Su JP, Zeng LL, et al. Gene expression and brain imaging association study reveals gene signatures in major depressive disorder. Brain Commun. 2024;6(4):fcae258. doi:10.1093/braincomms/fcae258
21. Das SC, Schulmann A, Callor WB, et al. Altered transcriptomes, cell type proportions, and dendritic spine morphology in hippocampus of suicide decedents. J Affect Disord. 2024;367:118-128. doi:10.1016/j.jad.2024.08.144
22. Goes FS, Collado-Torres L, Zandi PP, et al. Large-scale transcriptomic analyses of major depressive disorder reveal convergent dysregulation of synaptic pathways in excitatory neurons. Nat Commun. 2025;16(1):3981. doi:10.1038/s41467-025-59115-4
23. Francis A, Roy B, Dwivedi Y. Deconvolution-based transcriptomic analysis in the hippocampus reveals cell type-specific risk genes and pathways associated with depression and suicide. Biol Psychiatry Glob Open Sci. 2025;5(5):100530. doi:10.1016/j.bpsgos.2025.100530
24. Sahay S, Lundh AE, Sirole RP, et al. Purinergic system transcript changes in the dorsolateral prefrontal cortex in suicide and major depressive disorder. Int J Mol Sci. 2025;26(5):1826. doi:10.3390/ijms26051826
25. Arasappan D, Spears A, Shah S, et al. Brain transcriptomic signatures for mood disorders and suicide phenotypes: an anterior insula and subgenual ACC network postmortem study. Brain Behav Immun Health. 2025;48:101051. doi:10.1016/j.bbih.2025.101051
26. Hwang A, Skarica M, Xu S, et al. Single-cell transcriptomic and chromatin dynamics of the human brain in PTSD. Nature. 2025;643(8072):744-754. doi:10.1038/s41586-025-09083-y
27. Gerstner N, Fröhlich AS, Matosin N, et al. Contrasting genetic predisposition and diagnosis in psychiatric disorders: a multi-omic single-nucleus analysis of the human OFC. Sci Adv. 2025;11(10):eadq2290. doi:10.1126/sciadv.adq2290
28. Matan-Lithwick S, Misztal MC, Yang M, et al. A transcriptomic signature of depressive symptoms in late life. Biol Psychiatry Glob Open Sci. 2025;5(3):100448. doi:10.1016/j.bpsgos.2025.100448
29. Wang M, Xiang H, Wei J, et al. Identification of blood transcriptome modules associated with suicidal ideation in patients with major depressive disorder. Sci Rep. 2025;15(1):1067. doi:10.1038/s41598-025-85431-2
30. Yan M, Chen M, Jiang Q, et al. A network analysis of gene co-expression in post-mortem brain tissues identifying novel genes and biological pathways underlying major depression. Front Psychiatry. 2025;16:1556983. doi:10.3389/fpsyt.2025.1556983
31. Francis A, Dwivedi Y. Multiomic single-nucleus profiling reveals cell-type-specific epigenetic and transcriptional dysregulation in major depressive disorder brain. Int J Neuropsychopharmacol. 2026;29(9):pyag045 doi:10.1093/ijnp/pyag045
32. Gao R, Otsuka I, Shirai T, et al. Postmortem brain single-nucleus and bulk gene expression analyses identify shared and distinct abnormalities in bipolar disorder and major depressive disorder. Transl Psychiatry. 2026;16(1):442. doi:10.1038/s41398-026-04200-5
33. Langfelder P, Horvath S. WGCNA: an R package for weighted correlation network analysis. BMC Bioinformatics. 2008;9:559. doi:10.1186/1471-2105-9-559